Turkish Journal of Electrical Engineering & Computer Sciences

http://journals.tubitak.gov.tr/elektrik/

Research Article

Turk J Elec Eng & Comp Sci
(2017) 25: 4341 – 4353

doi:10.3906/elk-1702-175

Indirect adaptive neurofuzzy Hermite wavelet based control of PV in a grid-connected hybrid power system

Sidra MUMTAZ, Laiq KHAN*
Department of Electrical Engineering, COMSATS Institute of information Technology, Abbottabad, Pakistan

Received: 14.02.2017 • **Accepted/Published Online:** 28.04.2017 • **Final Version:** 05.10.2017

Abstract: Owing to the evolution of the smart grid, the emergence of hybrid power systems (HPSs), and the proliferation of plug-in-hybrid electric vehicles, the development of efficient and robust maximum power point tracking (MPPT) algorithms for renewable energy sources due to their inherent intermittent nature has overwhelmed the power industry. In this paper, an incremental conductance (IC) based Hermite wavelet incorporated neurofuzzy indirect adaptive MPPT control paradigm for a photovoltaic (PV) system in a grid-connected HPS is proposed. The performance of the proposed adaptive Hermite wavelet incorporated neurofuzzy MPPT control paradigm is validated through a comprehensive grid-connected HPS test-bed developed in MATLAB\Simulink by comparison with an IC based adaptive indirect neurofuzzy Takagi–Sugeno–Kang (TSK) control scheme, IC based adaptive direct neurofuzzy TSK control system, IC based adaptive proportional-integral-derivative (adapPID) control scheme, and IC algorithm for PV systems.

Key words: Photovoltaic, maximum power point tracking, neurofuzzy, Hermite wavelet, hybrid power system

1. Introduction

Energy demand is continuously increasing all over the world on one hand and conventional energy resources (fossil fuels) are depleting with the passage of time on the other hand. Moreover, these fossil fuels are not only very expensive but also emit enormous amounts of greenhouse gases and auxiliary pollutants. To increase the diversity in the energy market, decrease the global atmospheric emissions, and obtain the long-term sustainable supplies, the need for alternative energies grows with time.

Renewable energy is clean and sustainable and it never runs out. Among numerous renewable energy sources, photovoltaic (PV) energy is the fastest growing resource due to its paramount availability. As PV energy is highly intermittent in nature and its power generation capability depends upon meteorological conditions, i.e. irradiance and temperature, the voltage and current of PV panels need to be controlled for maximum power extraction. In order to enhance the output efficiency, PV energy is operated at its maximum power point, which needs a great effort. Change in solar irradiance or temperature alters the maximum power point of a PV energy system; therefore, the MPPT algorithm is used to keep the system at the highest power point [1].

In the literature, different conventional and intelligent MPPT tracking algorithms have been used to enhance convergence, control, and stability and minimize cost [2,3]. Conventional techniques like perturb and observe (P&O), hill climbing (HC), incremental conductance, open circuit voltage (OCV), or short circuit current (SCC) are widely used in the literature. P&O and HC MPPT algorithms are extensively used due to

*Correspondence: laiq@ciit.net.pk

their simplicity and ease of implementation [4,5]. These algorithms continuously track the peak power of a PV panel with the perturbation of voltage; however, these techniques are slow and get confused due to quick variations of atmospheric conditions. The shortcomings of the P&O and HC methods are overcome in the IC technique but it is complex to some extent and instability occurs in the expected output [6]. As in the OCV [7] and SCC techniques [8], the value of the proportionality constant depends upon the PV panel aging, so the performance degrades with the passage of time.

Recently, intelligent algorithms such as evolutionary algorithms, artificial neural networks (ANNs), fuzzy logic, and their hybrids are getting great attention. Evolutionary algorithms, e.g., the genetic algorithm (GA), particle swarm optimization (PSO), and ant colony optimization (ACO), have proven to be quite successful in tracking the maximum power point of PV energy [9,10]. These algorithms show robust behavior in low irradiance and/or partial shading conditions but the convergence speed, solution archive, and suitable selection of control parameters are still potential areas of concern. The ANN is a quite successful method for tracking the MPPT of PV systems, because the trained ANN provides the accurate MPPT without acquiring exhaustive knowledge about the PV parameters [11]. As PV energy is intermittent and a time-varying energy source, the ANN needs to be trained periodically for the PV array with which it is used. A fuzzy logic MPPT controller is one of the most promising control strategies for the unpredictable and nonlinear PV system but it requires a priori knowledge of the system input/output relationship [12].

The shortcomings of ANNs and fuzzy logic are overcome by hybridizing the ANN and fuzzy logic [13]. Neurofuzzy combines the explicit knowledge of fuzzy logic, which is explained and understood with the implicit knowledge of the ANN, which is acquired by learning [14]. However, neurofuzzy suffers from the inherent problems of getting stuck in local minima of the search space and low convergence speed. Likewise, the conventional neurofuzzy system has a linear consequent part, which makes it unable to cope with system nonlinearities. The limitations of the neurofuzzy system are overcome by introducing wavelets in its consequent part [15]. The multiresolution property of wavelets is used to investigate the nonstationary signals to find out their local details with high accuracy [16].

To address all of the abovementioned hitches, an efficient Hermite wavelet incorporated neurofuzzy indirect adaptive controller (HWNIAC) for MPPT of a PV system integrated with a HPS is proposed. In the stated HPS, tracking the maximum power point (MPP) is a quite challenging issue, because this system is highly characterized by nonlinearity. The nonlinearity occurs due to the unpredictable load, uncertain smart charging station load, dynamic solar radiation, and varying temperature. The HWNIAC not only tracks the MPPT of the PV system efficiently but also ensures the power quality recommended by the power industry.

The goals of this research work are:

- To develop a simulation test-bed in MATLAB/Simulink for a grid-connected HPS having energy sources (PV, solid oxide fuel cell (SOFC), electrolyzer, microturbine (MT), battery and supercapacitor (SC)), complex residential load, and a smart charging station (CS) for PHEVs.
- To formulate a HWNIAC for the PV system.
- To design a supervisory control system (SCS) for the hybrid power system.

The rest of the paper is organized into four main sections. Section 2 gives the details of system configuration and the PV model description. Section 3 gives the details of the proposed adaptive control

system design. Simulation results are discussed in Section 4. Section 5 concludes the outcomes of this research work.

2. System configuration and PV model description

The proposed hybrid power system consists of the PV, SOFC, electrolyzer, MT, and utility grid as sources and residential load as a demand and the PHEVs' CS as a source and load, both as shown in Figure 1.

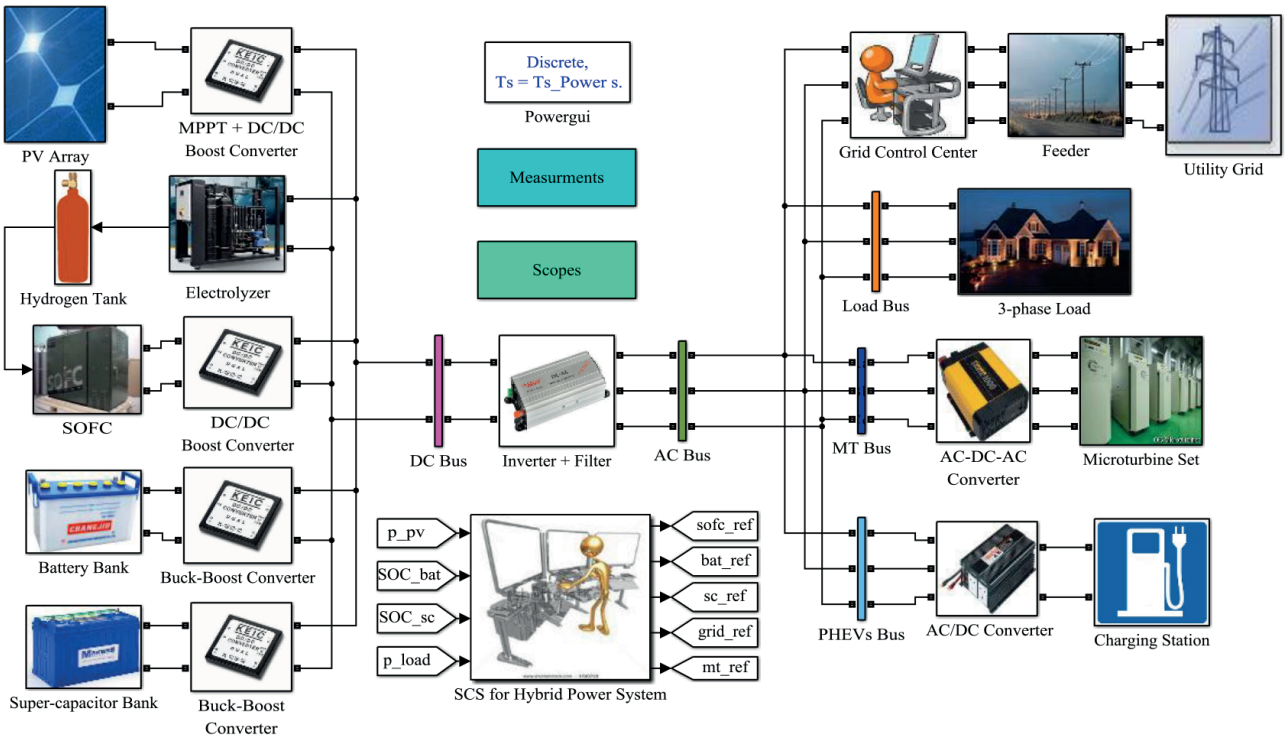

Figure 1. Hybrid power system Simulink test-bed.

The PV is connected to a DC bus via a DC/DC converter, which comprises two cascaded converters. The DC/DC boost converter is used to boost up the PV output voltage to the DC bus voltage. The DC bus voltage must be kept constant to avoid the creation of harmonics. In the SOFC system, the boost converter is connected to a voltage regulator, which regulates the output voltage of the SOFC to the DC bus voltage. The excess power generated by renewable energy sources is given to the electrolyzer via the DC/DC converter to produce hydrogen. The MT is connected to an AC bus via an AC/DC/AC converter. The AC power output of the MT is quite difficult to control, because high frequency (1600 Hz) AC output needs to be converted (50 Hz) for general use. The main inverter used in the HPS interconnects or shares power between the renewable energy sources and loads/grid. The battery and SC are connected to the DC bus through a DC/DC buck-boost converter followed by a DC voltage regulator. A CS for PHEVs is connected to an AC bus. PHEVs have the potential to transmit auxiliary power back to the grid during peak hours. Thus, the CS manages the bidirectional flow of power between the utility grid and PHEVs. A battery storage system (BSS) is used in the charging station to store the excess power either from HPS or PHEVs.

2.1. PV model

The PV cell voltage and current alter with the change in solar radiation and atmospheric temperature. The PV array current can be calculated as follows:

$$I_{pv} = I_{light} - I_d - \frac{V_d}{R_{shunt}} \tag{1}$$

Here, I_{pv} is the PV array generated current, I_{light} is incident light current, I_d is the diode current, and V_d is the diode voltage. The voltage of the PV array is calculated as:

$$V_{pv} = n_s \left(\frac{\alpha\tau T}{q}\right) \ln\left\{\frac{I_s - I_{pv} + n_p}{n_p \tilde{I}}\right\} - \frac{n_s}{n_p} I_{pv} R \tag{2}$$

Here, V_{pv} is the PV array voltage, n_s is the number of series-connected cells, n_p is the number of parallel-connected cells, T is cell temperature, α is the temperature coefficient, τ is Boltzmann's constant, q is the charge of an electron, I_s is the short circuit current, $\hat{I}$ is the diode saturation current, and R is series-connected resistance.

2.2. Proposed adaptive control system design for PV

The PV system produces the current I_{pv} when solar radiations fall on it. The terminal voltage, V_{pv}, appears at the output of the PV system, which is given by Eq. (2). For any solar irradiance, the MPP is unique and this MPP gives the maximum output power of the PV system. The MPP is achieved as:

$$s = \frac{\partial P_{pv}}{\partial V_{pv}} = \frac{\partial\left(I_{pv} \times V_{pv}\right)}{\partial V_{pv}} = I_{pv}\frac{\partial V_{pv}}{\partial V_{pv}} + V_{pv}\frac{\partial I_{pv}}{\partial V_{pv}} = \frac{I_{pv}}{V_{pv}} + \frac{\partial I_{pv}}{\partial V_{pv}} = 0 \tag{3}$$

Eq. (3) is solved to compute the voltage at the MPP at every instant of time using the MPPT algorithm subject to the following assumption:

$$\text{Assumption:} \begin{cases} THD_V < 5\% \\ \quad -6\%V_{rms} < V_{rms} < +6\%V_{rms} \\ P_{gen} + P_{mt} \pm P_{grid} = \pm P_{cs} + P_{load} \\ Q_{gen} + Q_{mt} \pm Q_{grid} = \pm Q_{cs} + Q_{load} \end{cases}$$

The MPPT problem here is to estimate the MPP of the PV system for varying solar irradiance and temperature by applying the MPPT algorithm. The MPPT algorithm makes the PV system operate at the estimated MPP. The MPPT algorithm must be quite efficient so that maximum power conversion efficiency is achieved. THD_v is the total harmonic distortion for load voltage. THD_V evaluates the quality of output AC signal and is calculated as:

$$THD_v = \sqrt{\sum_{i=2}^{n} V_i^2 \Big/ V_f} \tag{4}$$

Here, f =50 Hz is the fundamental frequency. THD_V and V_{rms} are taken as HPS performance indexes. V_{rms} is load rms voltage and the acceptable variations in V_{rms} are up to 6%. P_{mt}, P_{grid}, P_{cs}, and P_{load} are the

average active powers of the MT, grid, CS, and load. $Q_{mt}, Q_{grid}, Q_{cs},$ and Q_{load} are the average reactive powers of the MT, grid, CS, and load. The average active power P and average reactive power Q are calculated as:

$$P = \frac{1}{2} V_m I_m \cos(\theta_V - \theta_I) \quad \& \quad Q = \frac{1}{2} V_m I_m \sin(\theta_V - \theta_I) \tag{5}$$

Here, V_m and I_m are the amplitude of voltage and current for the respective source or load. Power from renewable energy sources is $P_{gen} = P_{pv} \pm P_{sc} \pm P_{bat} + P_{sofc} - P_{elect}$. Here, P_{sc}, P_{bat}, and P_{elect} are output average active powers of the SC, battery, and electrolyzer, respectively.

2.3. Hermite wavelet incorporated neurofuzzy identifier

A Hermite wavelet incorporated neurofuzzy identifier (HWNI) is used to identify the PV system. The Hermite wavelet is proven very effective and robust to solve nonlinear problems, so the Hermite wavelet is introduced for the interval [0, 1] in the consequent part of the proposed neurofuzzy network and is given as:

$$\psi_{n,m}(x) = \begin{cases} 2^{k/2}\sqrt{\frac{2}{\pi}} H_m(2^k x - 2n + 1), & \frac{n-1}{2^{k-1}} \le x \le \frac{n}{2^{k-1}} \\ 0 & \text{Otherwise} \end{cases} \tag{6}$$

Here, x is the input; k is the positive integer, which represents the level of resolution; $n = 1, \cdots, 2^{k-1}$ is the translation factor; and $m = 1, \cdots, M-1$ is the degree of the polynomial. H_m is the Hermite polynomial of degree m defined for the interval $H_m = [-\infty, +\infty]$ and $H_0(x) = 1, \quad H_1(x) = 2x$ and $H_{m+1}(x) = 2xH_m(x) - 2mH_{m-1}(x)$. The adaptive neurofuzzy network consists of seven layers as shown in Figure 2. The fuzzy inference system consists of IF-THEN rules in its antecedent part.

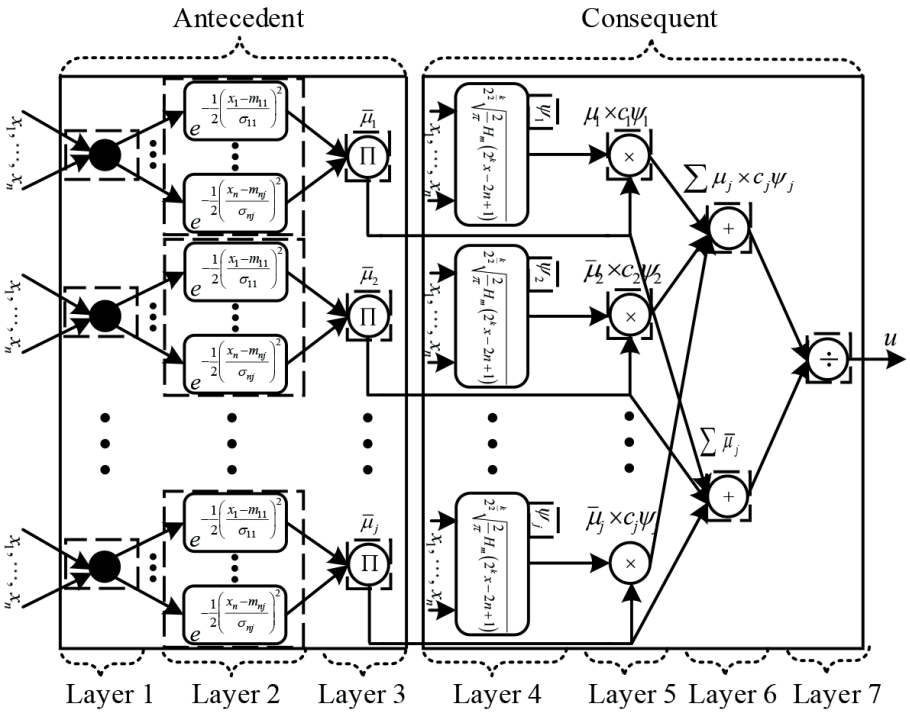

Figure 2. Configuration of neurofuzzy network.

$$R_j : \; if \; x_1 \; is \; \mu_{1\,j}, \; x_{\,2} \; is \; \mu_{2j}, \; \cdots, \; x_{nj} \; is \; \mu_{nj}, \; then \; y = \psi_j$$

Here, x_n is the input linguistic variable, μ_{nj} is the fuzzy set corresponding to x_n, and y is the network output variable. j is the number of rules, $j = 1, \cdots, J$ and J is the number of existing rules. The function of each layer is explained as follows:

Layer 1: This layer receives the input values.

Layer 2: This layer is called the fuzzification layer. The Gaussian membership function is used to compute the linguistic terms for each input as follows:

$$\mu_{ij} = e^{\frac{-1}{2}\left[\frac{x_i - m_{ij}}{\sigma_{ij}}\right]^2} \tag{7}$$

Here, m_{ij} and σ_{ij} are the mean and variance of the Gaussian membership function, respectively.

Layer 3: In this layer, the firing strength for each rule is calculated using the product T-norm.

$$\bar{\mu}_{ij} = \prod_{i=1}^{n} \mu_{ij} \tag{8}$$

Layer 4: Hermite wavelet functions are presented in this layer as follows:

$$\beta_j = \sum_{i=1}^{2^{k-1}} c_{ij} \psi_{ij}(x) \tag{9}$$

Layer 5: In this layer, the output of the antecedent (layer 3) and consequent (layer 4) parts are multiplied for each input and then they are added.

Layer 6: This layer calculates the sum of the output of layer 3.

Layer 7: The final output is computed in this layer and given as:

$$u = \frac{\sum_{i=1}^{n} \bar{\mu}_{ij} \beta_j}{\sum_{i=1}^{n} \bar{\mu}_{ij}} \tag{10}$$

The abovementioned wavelet based neurofuzzy network is proven as a universal approximator for continuous functions over compact sets. From Eq. (10), let $u = \hat{s}$, and then the error function, J_I, for the training of the HWNI is given as:

$$J_I = \frac{1}{2} \left(\hat{s}(k) - s(k)\right)^{\;2} \tag{11}$$

Parameters for the training algorithm are $\xi = [m_{ij}, \; \sigma_{ij}, c_{ij}]$. By applying the gradient descent method on the error function, the following update equation is obtained.

$$\xi(k+1) = \xi(k) + \alpha \left(\hat{s}(k) - s(k)\right) \frac{\partial \hat{s}(k)}{\partial \xi} \tag{12}$$

Applying the chain rule:

$$\frac{\partial \hat{s}(k)}{\partial m_{ij}} = \frac{\partial \hat{s}(k)}{\partial \bar{\mu}_j}\frac{\partial \bar{\mu}_j}{\partial \mu_j}\frac{\partial \mu_j}{\partial m_{ij}} = \left[\frac{\beta_j - \hat{s}(k)}{\sum_{j=1}^{n}\mu_j}\right]\mu_j\frac{(x_i - m_{ij})}{\sigma_{ij}^2} \tag{13}$$

$$\frac{\partial \hat{s}(k)}{\partial \sigma_{ij}} = \frac{\partial \hat{s}(k)}{\partial \bar{\mu}_j}\frac{\partial \bar{\mu}_j}{\partial \mu_j}\frac{\partial \mu_j}{\partial \sigma_{ij}} = \left[\frac{\beta_j - \hat{s}(k)}{\sum_{j=1}^{n}\mu_j}\right]\mu_j\frac{(x_i - m_{ij})^2}{\sigma_{ij}^3} \tag{14}$$

$$\frac{\partial \hat{s}(k)}{\partial c_{ij}} = \frac{\partial \hat{s}(k)}{\partial \beta_j}\frac{\partial \beta_j}{\partial c_{ij}} = \left[\frac{\mu_j}{\sum_{j=1}^{n}\mu_j}\right]\psi_j \tag{15}$$

2.4. Hermite wavelet incorporated neurofuzzy indirect adaptive controller

The proposed HWNIAC is shown in Figure 3 where **P** represents the hybrid power system, $\mathbf{I_{PV}}$ represents the identifier for the PV system, and **C** represents the controller. From Eq. (10), let $u = u_{pv}$, and then the cost function to update the HWNIAC parameters is given as:

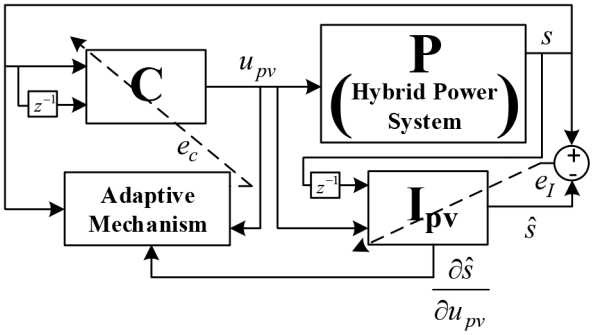

Figure 3. Closed-loop control system.

$$J_c = \frac{1}{2}\left[(r(k) - s(k))^2 + \lambda u_{pv}^2(k)\right] \tag{16}$$

Here, $r(k)$ is the known reference input and $s(k)$ is the plant output (PV system). u_{pv} is the control effort and λ is the learning rate used to adjust HWNIAC parameters. The generalized adaptive law to update the HWNIAC parameters is given as:

$$X(k+1) = X(k) + \eta\frac{\partial J_c(k)}{\partial X(k)} + \lambda\Delta e_c(k) \tag{17}$$

Here, $\Delta e_c(k) = \Delta\left(r(k) - s(k)\right)$, $X = [m_{ij},\ \sigma_{ij}, c_{ij}]$ is the adaptation vector for the HWNIAC and is calculated in the same way as in the HWNI. The term $\frac{\partial J_c(k)}{\partial X(k)}$ is simplified as:

$$\frac{\partial J_c(k)}{\partial X(k)} = \left[e_c(k)\frac{\partial \hat{s}}{\partial u_{pv}} - \lambda u_{pv}\right]\frac{\partial u_{pv}}{\partial X} \tag{18}$$

The term $\frac{\partial \hat{s}}{\partial u_{pv}}$ is calculated in the HWNI as follows:

$$\frac{\partial \hat{s}}{\partial u_{pv}} = \frac{\sum_{j=1}^{n} \mu_j \left[-\left(\frac{u_{pv} - m_{ij}}{\sigma_{ij}^2} \right) (\beta_j - \hat{s}) + 2\sqrt{\frac{2}{\pi}} \left\{ 8c_{11}^j + c_{12}^j (128u_{pv} - L) \right\} \right]}{\sum_{j=1}^{n} \mu_j} \tag{19}$$

The term L is calculated as: $\begin{cases} L = 32, & 0 \leq u_{pv} \leq 1/2 \\ L = 48, & 1/2 \leq u_{pv} \leq 1 \end{cases}$

2.5. Supervisory control system

Power management in the HPS is a prime issue. Due to a large number of renewable and nonrenewable energy sources, power distribution to the unpredictable load (residential and CS) may cause power quality and grid stability problems. To ensure a transfer of continuous, stable, and quality power to the load, the SCS is applied. In the SCS, PV is considered as the primary source from which maximum power is extracted to satisfy the load demand. The excess power is given to the electrolyzer to produce hydrogen and any scarcity of power is met by the SOFC and/or the battery. As the response of the battery is slow, to deal with transients, the SC is used to overcome the power shortage. The SCS ensures the consistent operation of all sources of the HPS and the continuous supply of power to the load. The operating modes for the SCS are:

- ***Mode 1 (surplus power):*** When PV generation is greater than the load, the surplus power is given to the battery and the SC for charging. If surplus power is still available, then it is given to the electrolyzer to produce hydrogen. The power balanced equation is written as:

$$P_{pv} = P_{load} + P_{elect} + P_{sc-c} + P_{bat-c}, \qquad P_{diff} > 0 \tag{20}$$

  Here, $P_{diff} = P_{pv} - P_{load}$, P_{sc-c} , and P_{bat-c} are the powers to charge the SC and battery.

- ***Mode 2 (deficient power):*** When PV generation is less than the load demand, then the battery delivers the power to overcome the shortage. If the battery is unable to satisfy the load, then the SC strives to reduce the power deficiency. If the SC is also incapable to compensate the power, then the SOFC delivers the power and attempts to overcome the scarcity. If a deficiency still exists, the power is taken from the utility grid, if it is available; otherwise, the MT is started to provide the remaining power. The overall balanced equation for deficient power is given as:

$$\left.\begin{aligned} P_{pv} &= P_{load} - P_{sc-d} - P_{bat-d} - P_{sofc} - P_{grid}, \quad t \neq peak\ hour \\ P_{pv} &= P_{load} - P_{sc-d} - P_{bat-d} - P_{sofc} - P_{mt}, \quad t = peak\ hour \end{aligned}\right\} \tag{21}$$

The complete flow of power management for the HPS is shown in Figure 4.

3. Simulation results and discussions

The HWNIAC is applied to a 265 kW PV system, which is the main source of the HPS. The Defense Housing Authority (DHA) of Islamabad, Pakistan, is considered as a case study, where the recorded coordinates are 33.7167° N, 73.0667° E. The irradiance and ambient temperature levels recorded by the regional meteorological station are taken for the longest day of the year, i.e. 22 June 2015, as shown in Figure 5.

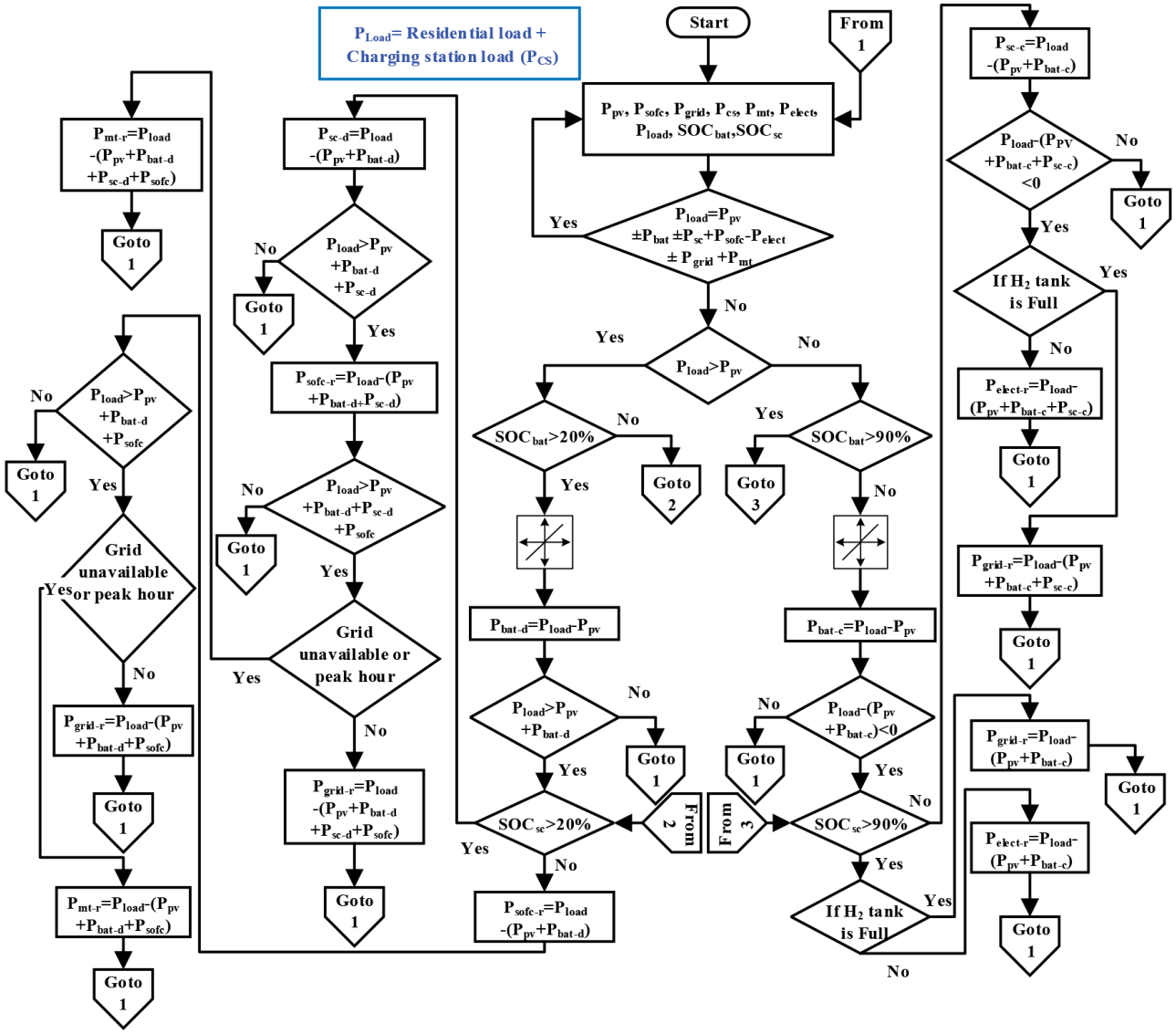

Figure 4. SCS work flow for HPS.

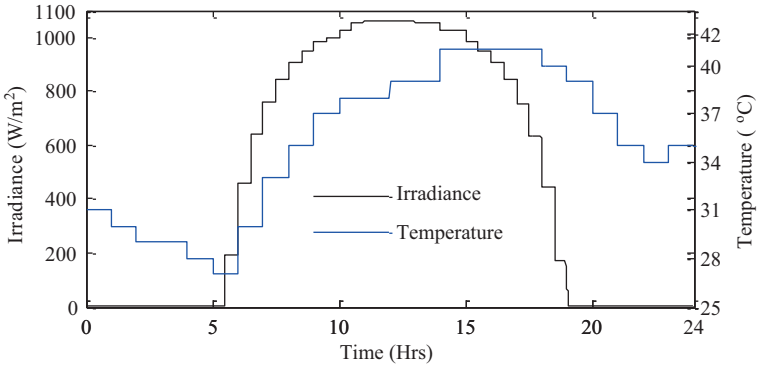

Figure 5. Irradiance and temperature levels for 22 June 2015.

The robustness of the HWNIAC is verified by achieving the MPPT of the PV system. It not only extracts the maximum power from the PV but also improves the overall performance of the system. The performance of the HWNIAC is compared with indirect neurofuzzy TSK, direct neurofuzzy TSK, and adapPID controllers in terms of overshoot, undershoot, steady state error, settling time, voltage regulation, and total harmonic distortion. Figure 6a shows that the reference power of PV is tracked by the HWNIAC, indirect neurofuzzy TSK, direct neurofuzzy TSK, adapPID, and IC algorithm for the PV system. The HWNIAC tracks the reference power with negligible overshoot and undershoot. The performance of the HWNIAC is superior to those of the other controllers, because, even under the rapid change in atmospheric conditions, the HWNIAC has negligible fluctuations, overshoot, undershoot, settling time, and steady state error, as presented in the Table. Figure 6b shows the MPPT error. The MPPT error is based on the principle of incremental conductance, i.e. the slope must be zero at the MPP. The HWNIAC quickly gets the MPP without losing its control, whereas, under the rapid change in irradiance level, other controllers are unable to rapidly track the MPP, which results in spikes. Although the HWNIAC, indirect neurofuzzy TSK, direct neurofuzzy TSK, and adapPID controllers are capable of attaining the MPP under varying atmospheric conditions, i.e. temperature and irradiance, the accuracy and stability achieved by the HWNIAC is better than that of the other controllers.

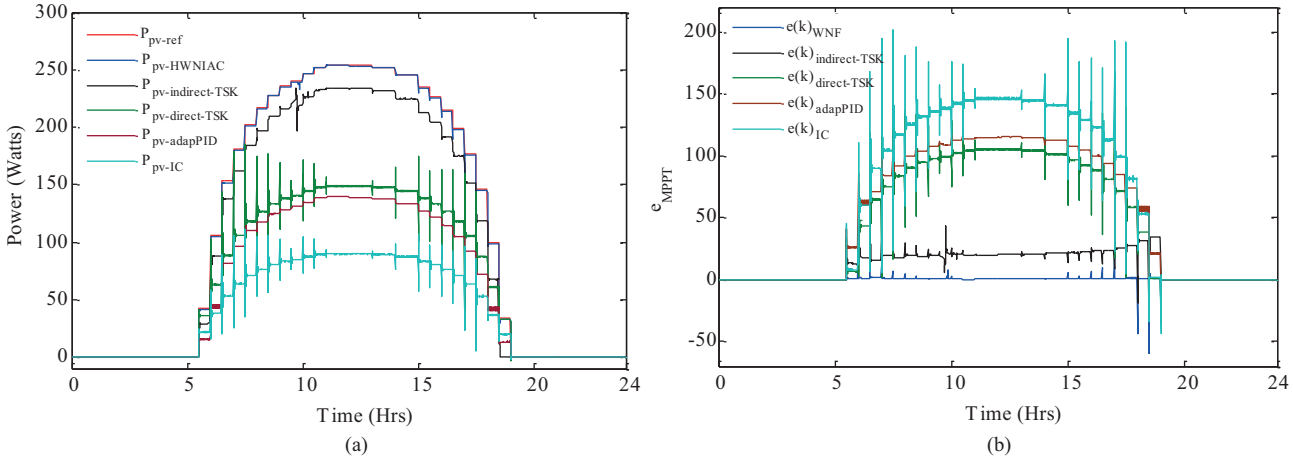

Figure 6. PV output power (a) and MPPT error (b).

Table. Comparative analysis of controllers.

Photovoltaic	HWNIAC	Indirect-TSK	Direct-TSK	adapPID	IC
Max. power (kW)	253.6	234	149	134	89
Overshoot	0%	6%	61%	4%	63%
Undershoot	–2%	–13%	–92%	0%	–90%
Steady state error (kw)	0.4	20	105	120	165
Settling time (s)	0.01	0.8	0.14	0.2	0.15
Max. deviation V_{rms}	0.2%	0.51%	1.232%	1.43%	1.84%
Max. deviation V_{THDs}	0.4%	1.226%	2.92%	3.45%	4.36%

The HWNIAC obtains maximum power from PV only during daytime. To satisfy the load, other sources of the HPS also play roles, which is addressed by the SCS. At nighttime, i.e. between 0 and 3.5 h, the load varies from 60 to 80 kW. During this time interval, PV is unable to provide the power due to the absence of solar irradiance. Due to the slow response of the SOFC system, the produced power slightly differs from the

reference power. Therefore, the initial tracking mismatch of the SOFC system is tried to be covered by the SC and battery. An overshoot is observed in SC power at t = 0 h, because the battery delivers the power according to the slew rate and the SC tries to meet the sudden change in load. The battery gives power up to 30 kW. During this time interval, the grid is available, so it delivers about 10 kW power. The MT is kept off, because the load is met by the SC, battery, and grid. For the interval of 3.5–6 h, the load varies from 80 to 120 kW. PV is unavailable up to 5.5 h, and after that it gives 40 kW. During this time interval, the SOFC system delivers 60–90 kW. The SC and battery are still in discharge mode. The grid delivers 17 kW power to cover the power deficiency. The MT is still kept off, because the load is met by the PV, SOFC, SC, battery, and grid. To keep the system stable, any access power is given to the electrolyzer to produce the hydrogen. During daytime, i.e. 6–18 h, the power scenario is completely different, because now maximum power (up to 250 kW) is taken from PV using the HWNIAC and delivered to the DC bus. During this time interval, PV satisfies the load. The surplus power generated by PV is used to charge the SC and battery. After charging the SC and battery, surplus power is given to the electrolyzer and then to the grid. The power given to the electrolyzer corresponds to the molar flow of hydrogen gas from the electrolyzer to the hydrogen tank. For 18–24 h, again PV is unavailable and the grid is already inaccessible due to peak load. The battery and SC are also in discharge mode but the load is still not satisfied. The SOFC delivers power up to 150 kW. The MT and CS provide the rest of the deficient power. The SCS makes sure that all the energy sources like the PV, MT, SOFC, SC, battery, and utility provide power according to the demand. In Figure 7, load active and reactive powers are shown. The reference power is the power required by the load. This reference power is adequately satisfied by the generating sources of the HPS.

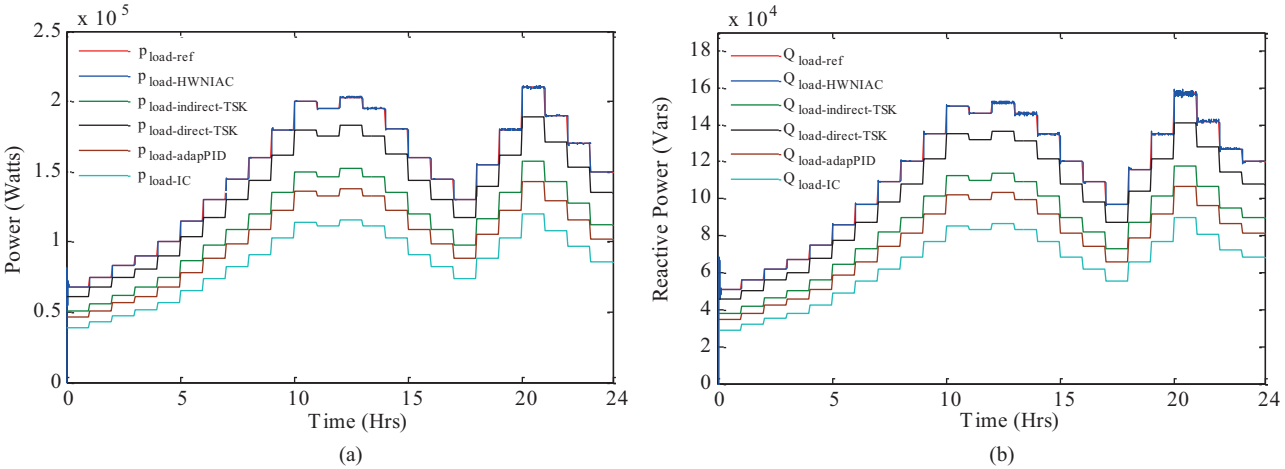

Figure 7. Load active (a) and reactive power (b).

Grid stability and power quality for the PV connected HPS are the two most important concerns for performance and life expectancy of the electrical equipment. To ensure the grid stability and power quality, assumptions are applied according to the IEEE 1547 standard [17]. Power quality is particularly addressed in the HPS, which is clearly shown in Figure 8. Load RMS voltage and THD for voltage are all in their acceptable limits, which ensures that the system is quite stable.

In order to compare the control system performance, various performance indexes, i.e. the integral time-weighted absolute error (ITAE), integral absolute error (IAE), integral time-weighted squared error (ITSE), and integral squared error (ISE), are computed. The HWNIAC indexes have the smallest and flattest profile, as

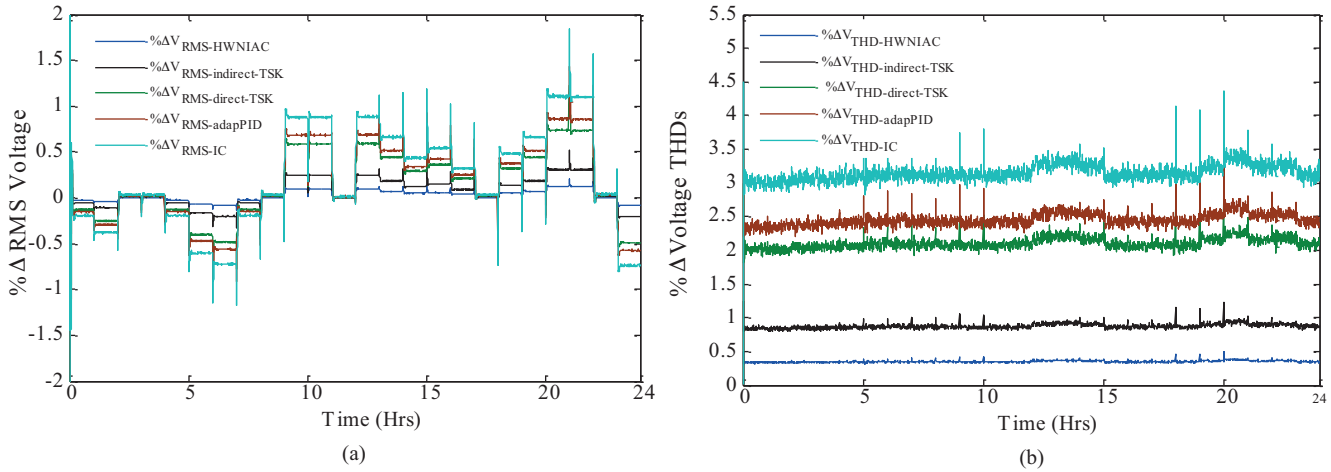

Figure 8. Percentage change in load rms voltage (a) and voltage THDs (b).

shown in Figure 9. The HWNIAC can track with a more stable output PV power as compared to other control schemes.

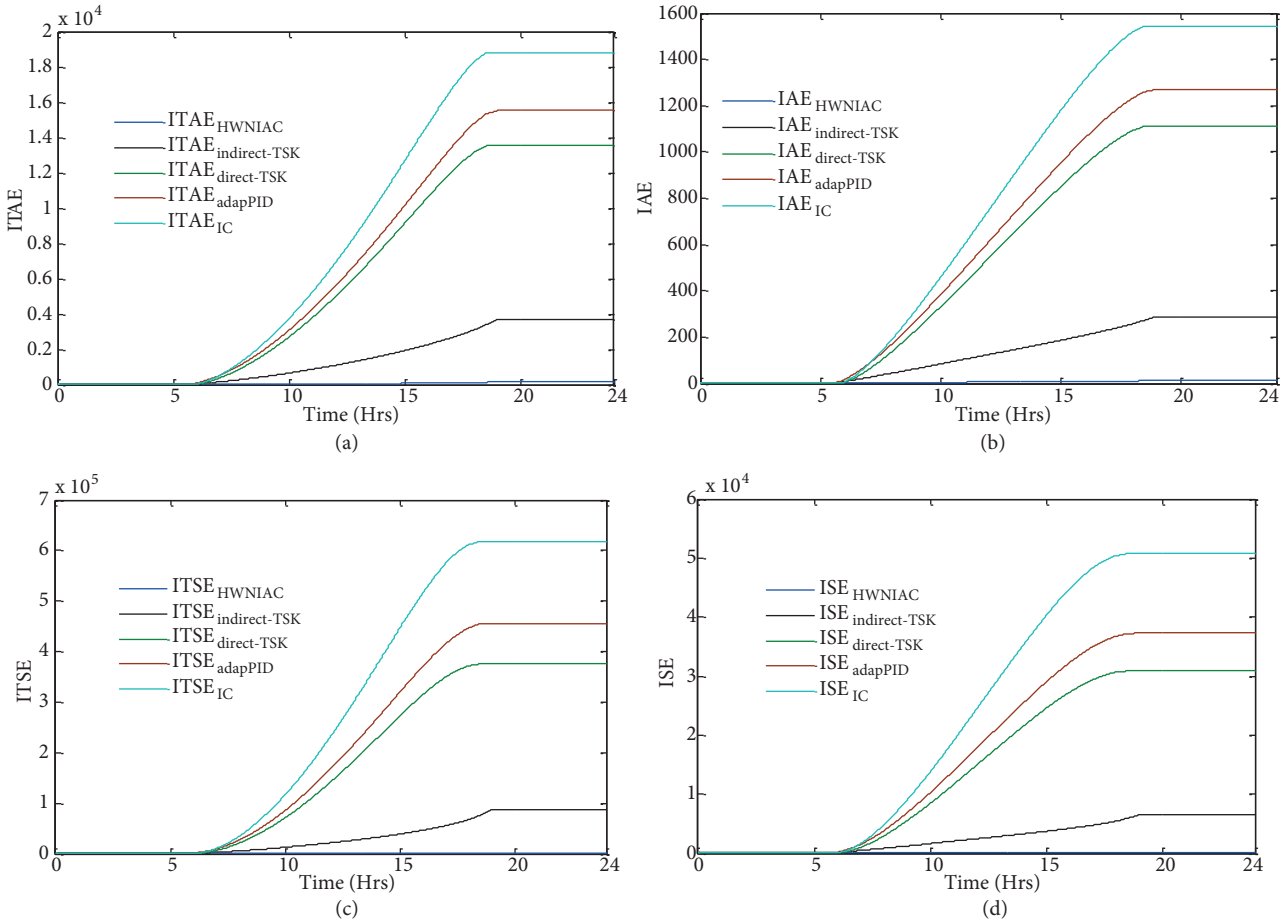

Figure 9. Performance indexes (ITAE (a), IAE (b), ITSE (c), and ISE (d)).

4. Conclusions

This paper presents the application of the HWNIAC for a PV system integrated with the HPS, which also includes a charging station for PHEVs. In order to achieve the reliable operation of the HPS, generated and consumed power is efficiently managed by the SCS. The HWNIAC works on the principle of incremental conductance. The HWNIAC not only tracks the MPPT of the PV system efficiently but also ensures the power quality recommended by the power industry. The performance of the proposed control scheme is analyzed in terms of overshoot, undershoot, settling time, steady state error, voltage regulation, and total harmonic distortion. Comparison of the HWNIAC with indirect neurofuzzy TSK, direct neurofuzzy TSK, adapPID, and IC indicates that the proposed MPPT control strategy outperforms the other control schemes.

References

[1] Eltawil MA, Zhao Z. MPPT techniques for photovoltaic applications. Renew Sust Energ Rev 2013; 25: 793-813.

[2] Reisi AR, Moradi MH, Jamasb S. Classification and comparison of maximum power point tracking techniques for photovoltaic system: a review. Renew Sust Energ Rev 2013; 19: 433-443.

[3] Esram T, Chapman PL. Comparison of photovoltaic array maximum power point tracking techniques. IEEE T Energy Conver 2007; 22: 439-449.

[4] Fermia N, Granozio D, Petrone G, Vitelli M. Predictive and adaptive MPPT perturb and observe method. IEEE T Aero Elec Sys 2007; 43: 934-950.

[5] Kjær SB. Evaluation of the "hill climbing" and the "incremental conductance" maximum power point trackers for photovoltaic power systems. IEEE T Energy Conver 2012; 27: 922-929.

[6] Lin CH, Huang CH, Du YC, Chen JL. Maximum photovoltaic power tracking for the PV array using the fractional-order incremental conductance method. Appl Energy 2011; 88: 4840-4847.

[7] Gokmen N, Karatepe E, Ugranli F, Silvestre S. Voltage band based global MPPT controller for photovoltaic systems. Sol Energy 2013; 90: 322-334.

[8] Noguchi T, Togashi S, Nakamoto R. Short-current pulse-based maximum power point tracking method for multiple photovoltaic and converter module system. IEEE T Ind Electron 2002; 49: 217-223.

[9] Kulaksiz AA, Akkaya R. A genetic algorithm optimized ANN-based MPPT algorithm for a stand-alone PV system with induction motor drive. Sol Energy 2012; 86: 2366-2375.

[10] Adly M, Besheer AH. A meta-heuristics search algorithm as a solution for energy transfer maximization in stand-alone photovoltaic systems. Int J Elec Power 2013; 51: 243-54.

[11] Liu YH, Liu CL, Huang JW, Chen JH. Neural-network-based maximum power point tracking methods for photovoltaic systems operating under fast changing environments. Sol Energy 2013; 89: 42-53.

[12] Alajmi BN, Ahmed KH, Finney SJ, Williams BW. Fuzzy logic control approach of a modified hill-climbing method for maximum power point in micro-grid standalone photovoltaic system. IEEE T Power Electr 2011; 26: 1022-1030.

[13] Badar R, Khan L. Coordinated adaptive control of multiple flexible AC transmission systems using multiple-input-multiple-output neuro-fuzzy damping control paradigms. Electr Pow Compo Sys 2014; 42: 818-830.

[14] Khan L, Lo KL, Jovanovic S. Hybrid GA neuro-fuzzy damping control system for UPFC. COMPEL 2006; 25: 841-861.

[15] Khan L, Badar R. Hybrid adaptive neuro-fuzzy B-spline based SSSC damping control paradigm using online system identification. Turk J Elec Eng & Comp Sci 2015; 23: 395-420.

[16] Abiyev RH, Kaynak O. Identification and control of dynamic plants using fuzzy wavelet neural networks. IEEE Int Symp Intell 2008; 1295-1301.

[17] Basso TS, DeBlasio R. IEEE 1547 series of standards: interconnection issues. IEEE T Power Electr 2004; 19: 1159-62.